Research Update: Structural and transport properties of (Ca,La)$FeAs_2$ single crystal

F. Caglieris, A. Sala, M. Fujioka, F. Hummel, I. Pallecchi, G. Lamura, D. Johrendt, Y. Takano, S. Ishida, A. Iyo, H. Eisaki, H. Ogino, H. Yakita, J. Shimoyama, and M. Putti

Citation: APL Materials **4**, 020702 (2016); doi: 10.1063/1.4941277

View online: http://dx.doi.org/10.1063/1.4941277

View Table of Contents: http://aip.scitation.org/toc/apm/4/2

Published by the American Institute of Physics

Research Update: Structural and transport properties of (Ca,La)$FeAs_2$ single crystal

F. Caglieris,[1] A. Sala,[1,2,3] M. Fujioka,[4,5] F. Hummel,[6] I. Pallecchi,[1] G. Lamura,[1] D. Johrendt,[6] Y. Takano,[4] S. Ishida,[3] A. Iyo,[3] H. Eisaki,[3] H. Ogino,[2] H. Yakita,[2] J. Shimoyama,[2,7] and M. Putti[1]
[1]*CNR-SPIN and Università di Genova, Via Dodecaneso 33, I-16146 Genova, Italy*
[2]*Department of Applied Chemistry, The University of Tokyo, Bunkyo, Tokyo 113-8656, Japan*
[3]*National Institute of Advanced Industrial Science and Technology (AIST), Tsukuba, Ibaraki 305-8565, Japan*
[4]*National Institute for Materials Science (NIMS), Tsukuba, Ibaraki 305-0047, Japan*
[5]*Hokkaido University, Sapporo, Hokkaido 001-0020, Japan*
[6]*Ludwig-Maximilians-Universität München, Department Chemie, Butenandtstr. 5-13, 81377 München, Germany*
[7]*Department of Physics and Mathematics, Aoyama Gakuin University, 5-10-1 Fuchinobe, Chuo-ku, Sagamihara 252-5258, Japan*

(Received 16 December 2015; accepted 21 January 2016; published online 8 February 2016)

Structural and transport properties in the normal and superconducting states are investigated in a $Ca_{0.8}La_{0.2}FeAs_2$ single crystal with T_c = 27 K, belonging to the newly discovered 112 family of iron based superconductors. The transport critical current density J_c for both field directions measured in a focused ion beam patterned microbridge reveals a weakly field dependent and low anisotropic behaviour with a low temperature value as high as $J_c(B = 0) \sim 10^5$ A/cm^2. This demonstrates not only bulk superconductivity but also the potential of 112 superconductors towards applications. Interestingly, this superconducting compound undergoes a structural transition below 100 K which is evidenced by temperature-dependent X-ray diffraction measurements. Data analysis of Hall resistance and magnetoresistivity indicate that magnetotransport properties are largely dominated by an electron band, with a change of regime observed in correspondence of the onset of a structural transition. In the low temperature regime, the contribution of a hole band to transport is suggested, possibly playing a role in determining the superconducting state.
[http://dx.doi.org/10.1063/1.4941277]

The discovery in 2008 of superconductivity in LaFeAs(O,F)[1] with a transition temperature (T_c) of 26 K has triggered huge interest in the new iron-based superconductors (IBSs). Several iron pnictide families have been synthesized, such as the 1111 family— *RE*FeAs(O,F) (*RE* = rare earth-elements),[2–4] the 122 family— *AE*Fe_2As_2 (*AE* = alkaline-earth metals),[5,6] and the 111 family— *AE*FeAs.[7,8] These compounds, sharing FeAs layers which play the main part in the conducting properties, exhibit several common characteristics, such as the multiband nature and the same unconventional superconducting mechanisms. However, differences in the crystal structure and anisotropy may induce modifications in the electronic structures which might be crucial for the optimization of the superconducting properties. Nowadays, the record in T_c among the IBS is 58 K and is held by the 1111 family,[9] but 122 compounds with lower anisotropy and larger coherence length are less affected by fluctuations and have allowed quick progresses in wire and tape fabrication of IBS.[10]

Thus, the search for new IBS compounds is important not only to increase T_c but also to cast light on the superconducting mechanisms, as well as to provide further improvements in the application potential of these compounds.

A new type of IBS has been discovered in 2013, the so-called 112 type, having general formula $Ca_{1-x}RE_xFeAs_2$, with RE = La, Ce, Pr, Nd, Sm, Eu, and Gd.[11–13] The T_c is maximum for La

concentration ~0.16 ($T_c \sim 34$ K), it decreases with increasing La content and for La ≥ 0.25, superconductivity eventually disappears.[14] Recently, Kudo *et al.* have reported an increase of T_c up to 47 K for La-Sb co-doping, with optimum La and Sb concentrations around 0.12 and 0.1, respectively.[15]

Furthermore, *RE*-Co and *RE*-Mn (with *RE* = La, Pr) co-dopings have been tested, resulting in a sharpening of the superconducting transition in Co-doped samples and in the suppression of superconductivity in Mn-doped samples.[16] We note that 112 Ni-based pnictide compounds sharing similar crystal structure also become superconductors, but at much smaller temperatures $T_c \approx 4$ K.[17]

112 compounds exhibit a layered structure, made of alternate stacking of superconducting anti-fluorite Fe_2As_2 planes and metallic blocking layers composed of (Ca, La) planes and As_2 zigzag chains. They crystallize in a monoclinic structure $P2_1$ (No. 4) or $P2_1/m$ (No. 11), in contrast with the other IBS crystal structures that are usually tetragonal or orthorhombic. A monoclinic to triclinic phase transition has been evidenced at 58 K in the $Ca_{0.73}La_{0.27}FeAs_2$ non-superconducting compound and it has been argued that it disappears when superconductivity is stabilized by Co doping.[18] On the other hand, a phase diagram has been outlined in Ref. 19 for the $Ca_{1-x}La_xFeAs_2$ system, where antiferromagnetic (AFM) ordering below $T_N \approx 60$ K-70 K is shown to persist up to high doping levels and coexist microscopically with bulk superconductivity at the optimal doping x = 0.15 with $T_c \approx 35$ K. This is a pretty peculiar behaviour among IBS compounds, where superconducting and AFM ground states are in competition with each other. It has been theoretically predicted[20] that in the monoclinic phase, the As_2 zigzag chains generate an additional three-dimensional hole pocket and cone-like electron pockets. In particular, the former should be generated by As $1p_z$ orbitals, while the latter by As $1p_x$ and $1p_y$ orbitals. These structures have been investigated through angle resolved photoemission spectroscopy (ARPES).[18,21,22] In particular, in a superconducting $Ca_{0.9}La_{0.1}FeAs_2$ single crystal, Xu *et al.*[22] resolved one additional hole-like band around the zone centre and one more fast-dispersing band near the X point in the vicinity of the Fermi level, beside the three hole-like and two electron-like bands usually reported for IBS. Although it is accepted that these bands arise from the strong coupling between the FeAs layers and the As zigzag bond layers, their influence on the superconducting and normal state properties is still unclear.

In this work, we performed a detailed characterization of a $Ca_{1-x}La_xFeAs_2$ single crystal in order to extract information on the crystal structure and its relationship with superconducting and normal state properties. In particular, we measured structural properties down to low temperatures, resistivity, magnetoresistivity, Hall effect, upper critical fields, and transport critical current density and finally discussed their relationship.

Samples with the nominal composition of $Ca_{0.85}RE_{0.15}FeAs_2$ were prepared by high pressure synthesis described elsewhere.[13] On a powder sample, temperature-dependent X-ray diffraction (XRD) measurements in the temperature range of 10–300 K were performed using a Huber G670 diffractometer with Co-Kα_1 radiation. Figure 1(a) shows the Rietveld refinement plot at 300 K. For details about Rietveld refinement of X-ray data, see Section 1 of the supplementary material.[23] In

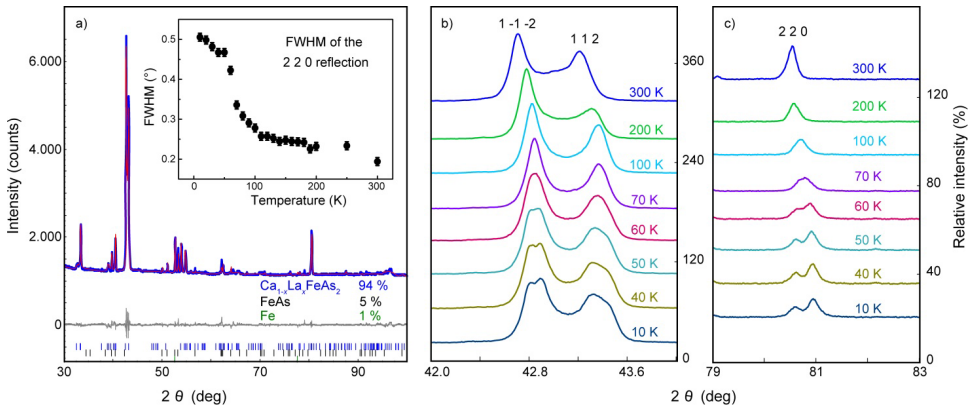

FIG. 1. (a) Rietveld refinement plot obtained for powder $Ca_{0.85}La_{0.15}FeAs_2$ sample at 300 K. Inset: Temperature dependence of the FWHM of the 220 diffraction peak. (b) and (c) Temperature evolution of the 1-1-2, 112, and 220 diffraction peaks, respectively.

Figures 1(b) and 1(c), the temperature-dependent behaviour of the 1-1-2, 112, and 220 diffraction peaks is reported. The sample undergoes a structural phase transition, indicated by the onset of a splitting of the 1-1-2, 112, and 220 reflections. This splitting can be explained by a transition from monoclinic to triclinic symmetry with all three angles unequal to 90°. Similarly, a structural transition is observed in other IBS.[24,25] In the inset of Figure 1, the plot of the full-width-half-maximum (FWHM) of the 220 reflection versus temperature shows that the transition onset is around 100 K, even if it may be considered complete at lower temperature $T \approx 60$ K.

A plate-like micrometric size single crystal extracted from the same batch was characterized using a scanning electron microscope (SEM) coupled with an electron dispersive spectrometer (EDS) for chemical analysis. The chemical composition obtained through EDS is $Ca_{0.76}La_{0.19}Fe_{0.98}As_{2.07}$ (in the following, indicated approximately as $Ca_{0.8}La_{0.2}FeAs_2$), corresponding to an La-content higher than the optimal doping condition.[11,15] The same crystal was subsequently shaped using a Focused Ion Beam (FIB) in order to obtain a slab of size 10 μm × 2 μm × 1 μm. Tungsten electrical contacts for the four-probe transport measurements were deposited by FIB as in Ref. 4, in the configuration shown in the inset of Figure 2 (left). The voltage electrodes V^+ and V^- were purposely misaligned in order to extract the longitudinal resistivity and the Hall effect by taking the even and odd parts of the signal with respect to the magnetic field, respectively.

Figure 2 (left) shows the resistivity, ρ, as a function of temperature. In the normal state, the resistivity curve follows a metallic trend in the mΩ cm range as in the case of other superconducting pnictides.[26–29] As magnified in Figure 2 (right), the superconducting transition is quite broad, exhibiting its onset at $T_c \approx 27$ K, while the zero-resistance is reached around $T_{c0} \approx 17$ K. The non-optimal T_c can be accounted for by the slight overdoping of this sample. The upper critical fields B_{c2} was evaluated from magnetoresistance measurements in the superconducting state, using the criterion of 90% of the normal state resistance, linearly extrapolated from T ≈ 36 K to below T_c. B_{c2} parallel and perpendicular to the c-axis are shown in Figure 2 (right). The slope $B'_{c2} = |\frac{dB_{c2}}{dT}|$ evaluated for B applied parallel and perpendicular to the c-axis is 2.0 T/K and 6.3 T/K, respectively. These values are similar to those found for the 1111 and 122 families[30] and indicate that the 112 compounds are large B_{c2} superconductors like other IBS. The B_{c2} anisotropy is around 3, in between the values ~2 typical of the 122 family[31,32] and ~5 of the 1111 family.[33,34] From the B_{c2} slopes, we calculated the Ginzburg-Landau (GL) coherence length in the directions parallel and perpendicular to the c-axis from the relations $B'^{\|c}_{c2} = \frac{\phi_0}{2\pi\xi^2_{ab}T_c}$ and $B'^{\perp c}_{c2} = \frac{\phi_0}{2\pi\xi_{ab}\xi_c T_c}$, respectively, obtaining the values and $\xi_{ab} \approx 2.5$ nm and $\xi_c \approx 0.8$ nm.

The critical current density J_c was extracted from transport measurements, as shown in Figure 3. Due to our micrometric geometry, J_c was evaluated using a 300 μV/cm criterion, corresponding to a voltage of ~0.06 μV that is unambiguously above the noise related to sensitivity of the nanovoltmeter ~nV (see voltage-current curves in the inset of Figure 3). With respect to the usual 1 μV/cm criterion, our 300 μV/cm criterion may overestimate the J_c values by nearly 10%. Figure 3 displays J_c as

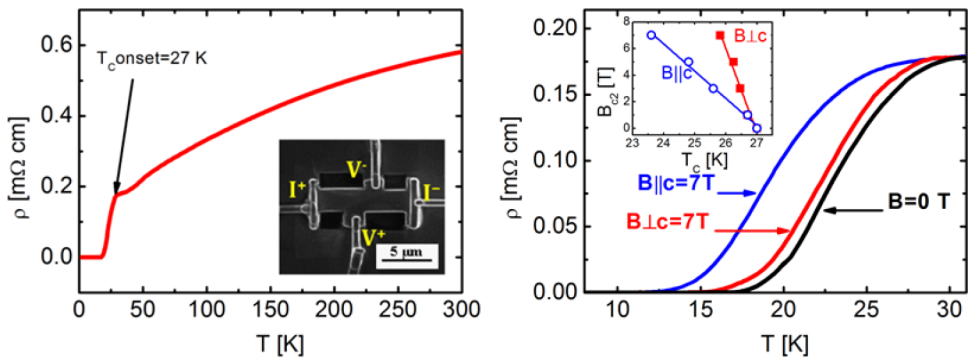

FIG. 2. Left: Resistivity vs T measurement of a $Ca_{0.8}La_{0.2}FeAs_2$ single crystal. Inset: FIB image of the FIB patterned crystal with the four probe configuration for transport measurements. Right: Resistivity transition for magnetic fields B = 0 and B = 7 T, applied both parallel (B||c) and perpendicular (B⊥c) to the c-axis. Inset: Upper critical field B_{c2} vs T_c up to B_{c2} = 7 T for applied magnetic field both parallel (B||c) and perpendicular (B⊥c) to the c-axis.

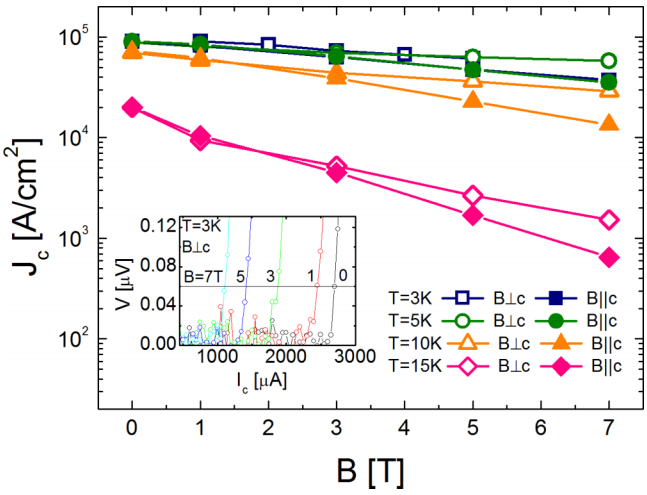

FIG. 3. Transport critical current density J_c measurements at fixed temperatures as a function of B, applied both parallel (B||c) and perpendicular (B⊥c) to the c-axis. Inset: V-I curves measured at T = 3 K at different perpendicular (B⊥c) fields. The continuous horizontal lines mark the threshold for the definition of J_c.

a function of the magnetic field at different temperatures with B applied both parallel and perpendicular to the c-axis. To the best of our knowledge, this is the first transport J_c report for the 112 family. The J_c value in self-field at the lowest temperatures is pretty high, around 10^5 A/cm^2 giving a strong confirmation of bulk superconductivity in our sample and more in general in 112 family. As in the other IBS, J_c is weakly affected by the magnetic field, remaining above 0.5×10^5 A/cm^2 for fields up to 7 T applied parallel to the c-axis. With increasing temperature up to 10 K, J_c is only weakly reduced (J_c values at 5 K are superimposed to those at 3 K), while a further increase to 15 K suppresses J_c substantially. Clearly, a certain sample inhomogeneity, responsible for the broadened resistive transition, also plays a role in the temperature decay of J_c as the temperature approaches the dissipative regime at T_{c0}. These results are comparable with the J_c values obtained from magnetization measurements[35] and also quite promising since they are only one order of magnitude lower than those measured on a FIB-patterned $SmFeAsO_{0.7}F_{0.25}$ single crystal.[36] The anisotropy $J_c^{B\perp c}/J_c^{B||c}$ turns out to be remarkably low, being lower than 1.5 at low temperatures, where the applied field is much smaller than B_{c2} in both directions.

In Figure 4 (left), we show the Hall coefficient R_H as a function of temperature. R_H is always negative and shows a non-monotonic behaviour ranging from -10×10^{-9} m^3/C at 30 K to -23×10^{-9} m^3/C at room temperature and exhibiting a broad maximum of -30×10^{-9} m^3/C around 150 K. These values are nearly ten times larger than the R_H values reported for 1111[26,27] and 122[28,29] superconducting compounds, suggesting that 112 compounds are further apart from the condition of charge

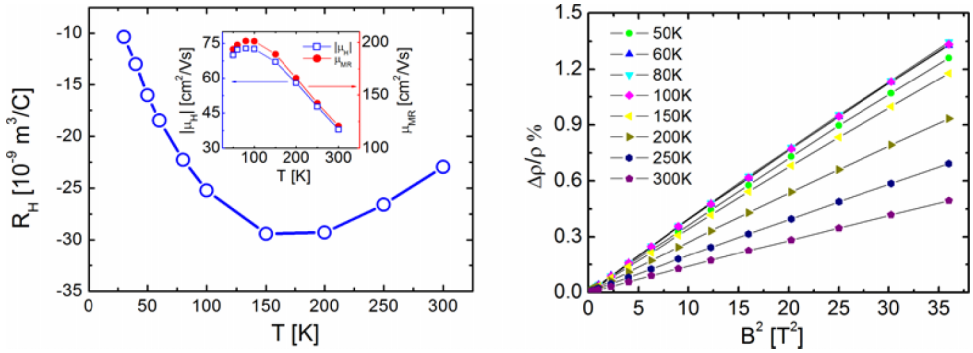

FIG. 4. Left: Hall effect R_H vs T measurement. Inset: Absolute value of Hall mobility ($|\mu_H|$) and effective carrier mobility (μ_{MR}) vs T. Right: Magnetoresistance $\Delta\rho/\rho$ vs B^2 measured at fixed temperature.

compensation typical of IBS, as also confirmed by the following analysis. The negative sign of R_H indicates that the main contribution to the conduction comes from an electron band, as expected from the La-doping and from the presence of As chains, where the formal As valence is −1 as opposed to −3 in Fe_2As_2 layers.[11,12] Indeed, both ARPES[18,21,22] and Density Functional Theory (DFT) calculations[20,37] reveal an extra electron pocket at the Brillouin zone edge (X point) of the Fermi surface originating from these As chains. However, the temperature dependence is somewhat unexpected; indeed, with decreasing temperature below 100 K, the absolute value of R_H decreases, while in other pnictide IBS families, it is either constant or increasing with decreasing temperature.[26–29]

Figure 4 (right) shows the magnetoresistance $\frac{\Delta\rho}{\rho} = \frac{\rho(B)-\rho(0)}{\rho(0)}$ as a function of B^2 at different temperatures in the normal state. All the curves show the parabolic behaviour expected from the standard cyclotron magnetoresistance mechanism. Interestingly, the temperature dependence is not trivial; indeed, $\Delta\rho/\rho$ increases with decreasing temperature from room temperature to 100 K, as usually $\Delta\rho/\rho$ does, but at lower temperatures, it remains constant and eventually decreases at the lowest temperature just above the superconducting transition.

As previously observed, also the Hall resistance is not monotonic. In order to explore the relationship between Hall effect and magnetoresistance behaviours in a multiband scenario, we calculated the Hall mobility $\mu_H = R_H/\rho$ which in a two-band system of electrons and holes is given by $\mu_H = \frac{R_H}{\rho} = \frac{\sigma_h\mu_h - \sigma_e\mu_e}{\sigma_h+\sigma_e} = \frac{\sqrt{\sigma_h\sigma_e}}{\sigma_h+\sigma_e}\left(\sqrt{\frac{\sigma_h}{\sigma_e}}\mu_h - \sqrt{\frac{\sigma_e}{\sigma_h}}\mu_e\right)$, where μ_e, μ_h are the carrier mobilities (both defined with positive sign, irrespective of the sign of the charge carriers) and σ_e, σ_h are the carrier conductivities. The cyclotron magnetoresistivity, to the leading order in B, can be written as $\Delta\rho/\rho \approx (\mu_{MR}B)^2$, where, in a two-band system, it is possible to define the effective carrier mobility as $\mu_{MR} = \frac{\sqrt{\sigma_h\sigma_e}}{\sigma_h+\sigma_e}(\mu_h + \mu_e)$.[38] The two mobilities may differ substantially in a two-band system with significantly different band conductivities, which is often the case in most of the compounds. Indeed, while μ_{MR} represents the average mobility of the two bands and does not contain information on the sign of the leading charge carriers, μ_H has the sign of the leading carriers and eventually becomes zero in a fully compensated system. In the inset of Figure 4 (left), we report μ_{MR} and $|\mu_H|$ as a function of temperature. It is interesting to note that (i) they exhibit the same temperature dependence in the whole temperature range; (ii) they increase with increasing temperature in the range 50–80 K, which is a rather anomalous behaviour and decrease with increasing temperature above 100 K, which is the more usual mobility behavior; and (iii) μ_{MR} is less than a factor three larger than $|\mu_H|$, while in multiband and nearly compensated systems, μ_{MR} might be one or two orders of magnitude larger than $|\mu_H|$.[38] These observations suggest that $Ca_{0.8}La_{0.2}FeAs_2$ is not close to charge compensation. Indeed, transport is dominated by the electron band in the whole temperature range and it can be roughly described in a single band framework. Above 100 K, the electron band mobility progressively decreases with temperature, as commonly observed. However, below 100 K-80 K, the anomalous increase of mobility with increasing temperature should be related to a change in the band structure around this temperature, likely to be related to the structural transition. We note that also the $\rho(T)$ curve shown in Figure 2 (left) and resistivity curves of others 112 compounds[12,13,15] exhibit a change of regime around the same temperatures. In the low temperature regime below ∼100 K, the system is still dominated by an electron band and also an hole band contributes appreciably to transport, as suggested by the trend of R_H that decreases in magnitude with decreasing T below ∼100 K. This scenario is confirmed by the two-band analysis of magnetotransport data presented in Section 2 of the supplementary material.[23] In particular, such hole band can be identified with the supplementary hole-like bands theoretically predicted[20,37] and observed by ARPES.[18,22]

In conclusion, we investigated structural and transport properties of a single crystal of the newly synthesized 112 family of IBS. Transport J_c measurements showed pretty high J_c values around 10^5 A/cm^2 at 3-5 K in self field, weakly dependent on the magnitude and orientation of the applied magnetic field, as in the other IBS. These results give a strong confirmation of bulk superconductivity for the 112 family. Remarkably, well stabilized superconductivity, evidenced by J_c and T_c values, is exhibited by the same sample undergoing a structural transition around 100 K, as evidenced by temperature dependent X-ray diffraction. This result is complementary with the recent finding of bulk superconductivity with $T_c \approx 35$ K and AFM ordering with $T_N \approx 62$ K co-existing in the same sample[19] and suggests that the structural and AFM transitions are related and

occur in the same temperature range. In Ref. 18, an analogous monoclinic-triclinic transition in the $Ca_{0.73}La_{0.27}FeAs_2$, not superconducting compound, is indeed found to be closely followed by a paramagnetic to stripe antiferromagnetic transition. Such observations are in sharp contrast with the usual phenomenology observed in superconducting iron pnictides, where full superconductivity establishes in the non-magnetic, tetragonal samples that do not exhibit phase transitions. Also, the Hall effect and magnetoresistivity measurements in the normal state revealed a different behavior in comparison with other IBS families with closely compensated multiband transport. The negative and quite large R_H values indicated that this compound is far away from being compensated and the main contribution to the conduction comes from an electron band, as expected from the La-doping and from the presence of As chains. The non-monotonic temperature dependence of mobilities extracted by Hall effect and magnetoresistivity, respectively, suggested that band structure rearrangement associated to the structural transition takes place below 100 K. Below this temperature, magnetotransport properties revealed the presence of the additional hole-like pockets theoretically predicted and observed through ARPES measurements, whose presence was related to the zigzag As chains. The understanding of the role of these chains and their coupling with the FeAs layers could be crucial to clarify how different block layers affect superconductivity in layered pnictides.

We acknowledge the support of the FP7 European project SUPER-IRON (Grant Agreement No. 283204), the CNR Seed Project (GAE: No. PGESE004), and the Japan Society for the Promotion of Science (JSPS).

[1] Y. Kamihara, T. Watanabe, M. Hirano, and H. Hosono, J. Am. Chem. Soc. **130**, 3296 (2008).
[2] Z. A. Ren, W. Lu, J. Yang, W. Yi, X. L. Shen, Z. C. Li, G.-C. Che, X. L. Dong, L. L. Sun, F. Zhou, and Z. X. Zhao, Chin. Phys. Lett. **25**, 2215 (2008).
[3] S. Matsuishi, Y. Inoue, T. Nomura, T. Yanagi, M. Hirano, and H. Hosono, J. Am. Chem. Soc. **130**, 14428 (2008).
[4] M. Fujioka, S. J. Denholme, M. Tanaka, H. Takeya, T. Yamaguchi, and Y. Takano, Appl. Phys. Lett. **105**, 102602 (2014).
[5] M. Rotter, M. Tegel, and D. Johrendt, Phys. Rev. Lett. **101**, 107006 (2008).
[6] K. Kudo, K. Iba, M. Takasuga, Y. Kitahama, J. Matsumura, M. Danura, Y. Nogami, and M. Nohara, Sci. Rep. **3**, 1478 (2013).
[7] J. H. Tapp, Z. Tang, B. Lv, K. Sasmal, B. Lorenz, P. C. W. Chu, and A. M. Guloy, Phys. Rev. B **78**, 060505(R) (2008).
[8] M. J. Pitcher, D. R. Parker, P. Adamson, S. J. C. Herkelrath, A. T. Boothroyd, R. M. Ibberson, M. Bruneli, and S. J. Clarke, Chem. Commun. **2008**, 5918–5920.
[9] M. Fujioka, S. J. Denholme, T. Ozaki, H. Okazaki, K. Deguchi, S. Demura, H. Hara, T. Watanabe, H. Takeya, T. Yamaguchi, H. Kumakura, and Y. Takano, Supercond. Sci. Technol. **26**, 085023 (2013).
[10] Y. Ma, Supercond. Sci. Technol. **25**, 113001 (2012).
[11] N. Katayama, K. Kudo, S. Onari, T. Mizukami, K. Sugawara, Y. Sugiyama, Y. Kitahama, K. Iba, K. Fujimura, N. Nishimoto, M. Nohara, and H. Sawa, J. Phys. Soc. Jpn. **82**, 123702 (2013).
[12] H. Yakita, H. Ogino, T. Okada, A. Yamamoto, K. Kishio, T. Tohei, Y. Ikuhara, Y. Gotoh, H. Fujihisa, K. Kataoka, H. Eisaki, and J. Shimoyama, J. Am. Chem. Soc. **136**, 846 (2014).
[13] A. Sala, H. Yakita, H. Ogino, T. Okada, A. Yamamoto, K. Kishio, S. Ishida, A. Iyo, H. Eisaki, M. Fujioka, Y. Takano, M. Putti, and J. Shimoyama, Appl. Phys. Express **7**, 073102 (2014).
[14] K. Kudo, T. Mizukami, Y. Kitahama, D. Mitsuoka, K. Iba, K. Fujimura, N. Nishimoto, Y. Hiraoka, and M. Nohara, J. Phys. Soc. Jpn. **83**, 025001 (2014).
[15] K. Kudo, Y. Kitahama, K. Fujimura, T. Mizukami, H. Ota, and M. Nohara, J. Phys. Soc. Jpn. **83**, 093705 (2014).
[16] H. Yakita, H. Ogino, A. Sala, T. Okada, A. Yamamoto, K. Kishio, A. Iyo, H. Eisaki, and J. Shimoyama, Supercond. Sci. Technol. **28**, 065001 (2015).
[17] A. Buckow, R. Retzlaff, J. Kurian, and L. Alff, Supercond. Sci. Technol. **26**, 015014 (2013).
[18] S. Jiang, C. Liu, H. Cao, T. Birol, J. M. Allred, W. Tian, L. Liu, K. Cho, M. J. Krogstad, J. Ma, K. M. Taddei, M. A. Tanatar, M. Hoesch, R. Prozorov, S. Rosenkranz, Y. J. Uemura, G. Kotliar, and N. Ni, e-print arXiv: 1505.0588.
[19] S. Kawasaki, T. Mabuchi, S. Maeda, T. Adachi, T. Mizukami, K. Kudo, M. Nohara, and G.-Q. Zheng, Phys. Rev. B **92**, 180508(R) (2015).
[20] X. Wu, C. Le, Y. Liang, S. Qin, H. Fan, and J. Hu, Phys. Rev. B **89**, 205102 (2014).
[21] Z.-H. Liu, T. K. Kim, A. Sala, H. Ogino, J. Shimoyama, B. Büchner, and S. V. Borisenko, Appl. Phys. Lett. **106**, 052602 (2015).
[22] L. Xu, L. De-Fa, Z. Lin, G. Qi, M. Qing-Ge, C. Dong-Yun, S. Bing, Y. He-Mian, H. Jian-Wei, H. Jun-Feng, P. Ying-Ying, L. Yan, H. Shao-Long, L. Guo-Dong, D. Xiao-Li, Z. Jun, C. Chuang-Tian, X. Zu-Yan, R. Zhi-An, and Z. Xing-Jiang, Chin. Phys. Lett. **30**, 127402 (2013).
[23] See supplementary material at http://dx.doi.org/10.1063/1.4941277 for details about Rietveld refinement of X-ray data and two-band analysis of magnetotransport data.
[24] H. Luetkens, H.-H. Klauss, M. Kraken, F. J. Litterst, T. Dellmann, R. Klingeler, C. Hess, R. Khasanov, A. Amato, C. Baines, M. Kosmala, O. J. Schumann, M. Braden, J. Hamann-Borrero, N. Leps, A. Kondrat, G. Behr, J. Werner, and B. Büchner, Nat. Mater. **8**, 305 (2009).
[25] E. Wiesenmayer, H. Luetkens, G. Pascua, R. Khasanov, A. Amato, H. Potts, B. Banusch, H.-H. Klauss, and D. Johrendt, Phys. Rev. Lett. **107**, 237001 (2011).
[26] M. Tropeano, I. Pallecchi, M. R. Cimberle, C. Ferdeghini, G. Lamura, M. Vignolo, A. Martinelli, A. Palenzona, and M. Putti, Supercond. Sci. Technol. **23**, 054001 (2010).

[27] P. Cheng, H. Yang, Y. Jia, L. Fang, X. Zhu, G. Mu, and H.-H. Wen, Phys. Rev. B **78**, 134508 (2008).
[28] M. Matusiak, Z. Bukowski, and J. Karpinski, Phys. Rev. B **83**, 224505 (2011).
[29] A. Olariu, F. Rullier-Albenque, D. Colson, and A. Forget, Phys. Rev. B **83**, 054518 (2011).
[30] M. Putti, I. Pallecchi, E. Bellingeri, M. R. Cimberle, M. Tropeano, C. Ferdeghini, A. Palenzona, C. Tarantini, A. Yamamoto, J. Jiang, J. Jaroszynski, F. Kametani, D. Abraimov, A. Polyanski, J. D. Weiss, E. E. Hellstrom, A. Gurevich, D. C. Larbalestier, R. Jin, B. C. Sales, A. S. Sefat, M. A. McGuire, D. Mandrus, P. Cheng, Y. Jia, H. H. Wen, S. Lee, and C. B. Eom, Supercond. Sci. Technol. **23**, 034003 (2010).
[31] C. Ren, Z.-S. Wang, H.-Q. Luo, H. Yang, L. Shan, and H.-H. Wen, Phys. Rev. Lett. **101**, 257006 (2008).
[32] A. Yamamoto, J. Jaroszynski, C. Tarantini, L. Balicas, J. Jiang, A. Gurevich, D. C. Larbalestier, R. Jin, A. S. Sefat, M. A. McGuire, B. C. Sales, D. K. Christen, and D. Mandrus, Appl. Phys. Lett. **94**, 062511 (2009).
[33] J. Jaroszynski, F. Hunte, L. Balicas, Y.-j. Jo, I. Raičević, A. Gurevich, D. C. Larbalestier, F. F. Balakirev, L. Fang, P. Cheng, Y. Jia, and H. H. Wen, Phys. Rev. B **78**, 174523 (2008).
[34] H.-S. Lee, M. Bartkowiak, J.-H. Park, J.-Y. Lee, Ju-Y. Kim, N.-H. Sung, B. K. Cho, C.-U. Jung, J. Sung Kim, and Hu-J. Lee, Phys. Rev. B **80**, 144512 (2009).
[35] W. Zhou, J. Zhuang, F. Yuan, X. Li, X. Xing, Y. Sun, and Z. Sh, Appl. Phys. Express **7**, 063102 (2014).
[36] P. J. W. Moll, R. Puzniak, F. Balakirev, K. Rogacki, J. Karpinski, N. D. Zhigadlo, and B. Batlogg, Nat. Mater. **9**, 628 (2010).
[37] J. H. Shim, K. Haule, and G. Kotliar, Phys. Rev. B **79**, 060501(R) (2009).
[38] M. Tropeano, M. R. Cimberle, C. Ferdeghini, G. Lamura, A. Martinelli, A. Palenzona, I. Pallecchi, A. Sala, I. Sheikin, F. Bernardini, M. Monni, S. Massidda, and M. Putti, Phys. Rev. B **81**, 184504 (2010).